Int. J. Electrochem. Sci., 13 **(2018)** 6608 – 6625, doi: 10.20964/2018.07.15

International Journal of
ELECTROCHEMICAL
SCIENCE
www.electrochemsci.org

Simulation and Experimental Investigation of Electrochemical Mill-grinding of GH4169 Alloy

Hansong Li[1,*], *Shuxing Fu*[1,2], *Shen Niu*[1], *Ningsong Qu*[1]

[1] College of Mechanical and Electrical Engineering, Nanjing University of Aeronautics and Astronautics, Nanjing 210016, China
[2] China Aviation Optical-Electrical Technology Co., Ltd., Luoyang 471003, China
[*]E-mail: hsli@nuaa.edu.cn

Received: 13 March 2018 / *Accepted:* 4 May 2018 / *Published:* 5 June 2018

Electrochemical mill-grinding (ECMG) is a new method of compound machining inspired by numerical-control milling. A simple rodlike grinding wheel that rotates at high speed is used as the cathode and processes the workpiece along a set trajectory. Electrochemical milling and grinding are both at play in ECMG, making it possible to machine large amounts of material from the workpiece while benefitting from excellent machining flexibility. In this paper, to machine GH4169 alloy highly efficiently, four types of rodlike grinding wheel are designed, all with a diameter of 10.2 mm, and the machining flow field is simulated using ANSYS software. The maximum feed rate of each grinding wheel is measured under different values of voltage and electrolyte pressure, and a groove-machining experiment is performed in which a maximum feed rate of 2.3 mm/min and material removal rate of 25.883 mg/s are achieved for a cutting depth of 10 mm. The machining accuracy and surface quality of the grooves are then compared and analysed.

Keywords: electrochemical mill-grinding; GH4169 alloy; feed rate; material removal rate

1. INTRODUCTION

GH4169 alloy is a nickel-based superalloy that has become an indispensable material in aircraft engines because of its high strength and good stability at high temperatures [1–3]. Because of the high strength, low thermal conductivity and strong work-hardening of GH4169 alloy, its cutting force, machining temperature and tool loss are very high [4–6], making GH4169 a typical difficult-to-machine material. Meanwhile, because electrochemical machining (ECM) is based on the principle of anode dissolution, no mechanical cutting force is generated [7–11]. This means that ECM is impervious to the strength and toughness of the material being machined, making it especially suitable for machining nickel-based superalloys.

Electrochemical milling is a new type of ECM that imitates the machining form of numerical-control milling. A simply shaped tool is used as the cathode, the trajectory of which is controlled by a computer to complete the ECM. Kozak et al. [12] used a bar-shaped cathode to process the surface of a workpiece in a form of electrochemical milling; a machined flat was obtained with a machining accuracy of ±0.02 mm and a surface roughness of 0.16–0.63 μm. Kozak et al. [13, 14] then established a mathematical model of surface electrochemical milling involving both ball-head and flat-plate cathodes. Hinduja et al. [15] studied the electrochemical milling of stainless steel 316 and compared the machining accuracies of using square and circular cathodes.

Electrochemical grinding (ECG) combines the advantages of ECM and grinding. It affords high machining accuracy and good grinding surface quality while also having the high efficiency of material removal of ECM for difficult-to-machine materials such as nickel-based alloys. By using ECG, Mahdavinejad et al. [16] achieved high-precision polishing of the inner surface of a complex workpiece, reducing the polishing time by a factor of 30 by optimizing the parameters. Tehrani et al. [17] studied the effect of a pulse voltage on ECG and explored the influence of different machining parameters on the degree to which the workpiece was overcut. By using a brazed diamond grinding wheel, Qu et al. [18] studied the influences of machining parameters on the feed rate and material removal rate (MRR) of Inconel 718 alloy.

To improve the flexibility of ECG, the electrochemical mill-grinding (ECMG) is presented by combining electrochemical milling with ECG. In ECMG, a simply shaped rodlike grinding wheel is used to machine a workpiece under the control of a computer. Li et al. [19, 20] studied the ECMG of GH4169 alloy. To increase the cutting depth, they used a hollow rodlike grinding wheel from inside which electrolyte was ejected; a feed rate of 2.6 mm/min was achieved at a cutting depth of 3 mm.

In the present study, to achieve a higher ECMG machining efficiency, four larger size hollow rodlike grinding wheels were designed and the machining flow field was simulated. The best grinding wheel was selected on the basis of the maximum feed rate, and a series of groove-machining experiments was conducted under different machining conditions. The machining accuracy and surface quality were then compared and analysed. The preferred machining effect was obtained by optimizing the experimental parameters.

2. SIMULATION ANALYSIS

2.1 Principle of ECMG

Fig. 1 shows ECMG schematically. The substrate of the grinding wheel is a hollow metal rod, the nickel-based diamond abrasive layer is fixed at the bottom of the rod and multiple electrolyte holes are distributed uniformly on the side wall of the grinding wheel. During machining, electrolyte is injected into the machining region from the hollow rod via the electrolyte holes. This structure ensures sufficient electrolyte in the machining region, discharges the processing products and Joule heat in a timely manner, reduces the occurrence of short circuiting and improves the stability of ECMG. The grinding wheel is connected to the positive pole, the workpiece is connected to the negative pole and the two are connected with the electrolyte of the machining region to form a circuit. To imitate milling, the grinding wheel is clamped on the rotating spindle of the milling machine and moved along the setting trajectory to machine the workpiece.

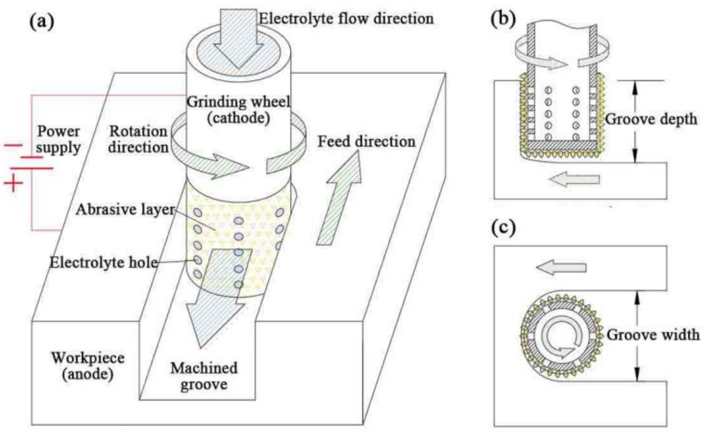

Figure 1. Schematic of ECMG. (a) 3D machining model. (b) Model side view. (c) Model top view.

Traditional ECG cannot achieve a large cutting depth because its electrolyte is injected into the machining region from outside. To achieve deeper cutting and higher MRR, four inner-jet grinding wheels (A/B/C/D) were designed in this study (Fig. 2). The number of holes in the bottom of grinding wheel A–D was 20, 30, 40 and 50, respectively, and the angle between two adjacent holes was 90°, 60°, 45° and 36°, respectively. The substrate of each grinding wheel was carbon steel 45, the outer diameter of the substrate was 10 mm, and the inter diameter was 8 mm. The diameter of the electrolyte hole on the side wall of the substrate was 1 mm. There were five layers of holes on each grinding wheel, and the distance from each layer to the bottom surface of the grinding wheel was 1.8 mm, 3.5 mm, 5.2 mm, 6.9 mm and 8.6 mm. The diamond abrasive particles were fastened on the substrate by electroplating, the size of the diamond particles was 75–90 μm, the diameter of each grinding wheel was 10.2 mm and the cutting depth was set as 10 mm.

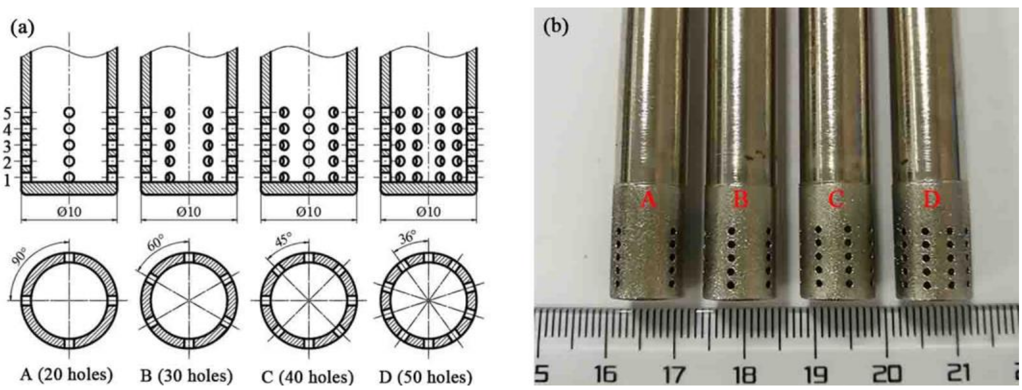

Figure 2. The four different grinding wheels used in this investigation. (a) Structure of grinding wheel. (b) Photograph of grinding wheel.

2.2 Flow-field simulation

In ECM, a change in the flow field can lead to a direct change in the surface quality and the machining precision of the workpiece. To simplify the calculation of the flow field in the machining region, we ignored the effect of the abrasive on the flow field. Fig. 3 shows the computational model of the electrolyte flow field in the machining region. The outer blue surface is that of the workpiece and the inner blue surface is that of the grinding wheel; both surfaces were set as walls in the simulation. The red region is the inlet for the electrolyte and was set as a pressure inlet. The green region is the outlet for the electrolyte and was set as a pressure outlet. According to previous processing experience, the side and bottom gaps in the model were all set to 0.2 mm. An observation section was set in the middle of the model to allow the flow field to be analysed easily. As shown in Fig. 4, a tetrahedral mesh was used to mesh the model, and the mesh in the gap was encrypted.

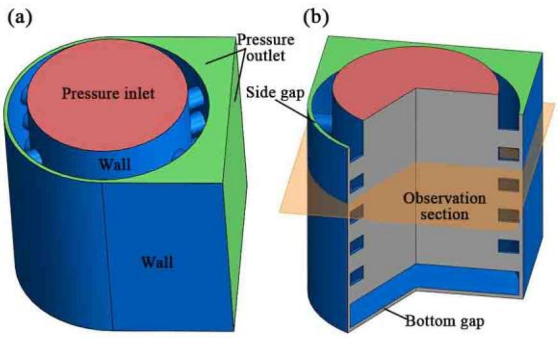

Figure 3. Simulation model of flow field. (a) Flow field model. (b) Model cutaway.

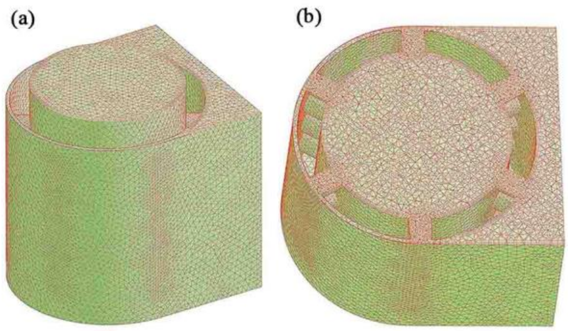

Figure 4. Mesh division of simulation model. (a) Model mesh. (b) Observation section mesh.

To simplify the complexity of calculating the electrolyte flow field in the machining region, we made the following assumptions: (i) the electrolyte was a viscous continuous incompressible fluid; (ii) during processing, the temperature was constant and no energy was lost; (iii) the flow field was no affected by bubbles or particles.

In ECMG, the flow of the electrolyte in the machining region is turbulent, the flow velocity varies greatly and the flow field is complex. We therefore used the standard k–ε turbulence model to simulate the flow field in the machining region, and the governing equations are as follows:

$$\frac{\partial(\rho k)}{\partial t}+\frac{\partial(\rho k u_i)}{\partial x_i}=\frac{\partial}{\partial x_j}\left[\left(\mu+\frac{\mu_t}{\sigma_k}\right)\frac{\partial k}{\partial x_j}\right]+G_k-\rho\varepsilon , \quad (1)$$

$$\frac{\partial(\rho \varepsilon)}{\partial t}+\frac{\partial(\rho \varepsilon u_i)}{\partial x_i}=\frac{\partial}{\partial x_j}\left[\left(\mu+\frac{\mu_t}{\sigma_\varepsilon}\right)\frac{\partial \varepsilon}{\partial x_j}\right]+C_{1\varepsilon}\frac{\varepsilon}{k}G_k-C_{2\varepsilon}\rho\frac{\varepsilon^2}{k} , \quad (2)$$

where k is the turbulent kinetic energy, ε is the turbulent dissipation rate, ρ is the density of the electrolyte, t is time, u_i is the flow speed in direction i, x_i (resp. x_j) is the displacement in direction i (resp. j), μ is the kinetic viscosity, the coefficients $C_{1\varepsilon}$ and $C_{2\varepsilon}$ equal 1.44 and 1.92, respectively, and the empirical constants σ_k and σ_ε equal 1 and 1.3, respectively. The turbulent kinetic energy generation term G_k and the turbulent viscosity μ_t are calculated from Eqs. (3) and (4), respectively:

$$G_k=\mu_t\left(\frac{\partial u_i}{\partial x_i}+\frac{\partial u_j}{\partial x_j}\right)\frac{\partial u_i}{\partial x_j} , \quad (3)$$

$$\mu_t=\rho C_\mu\frac{k^2}{\varepsilon} , \quad (4)$$

where u_j is the flow speed in direction j and coefficient C_μ is equal to 0.09.

We used the ANSYS FLUENT software to simulate the flow field. First, we explored how changing the number of electrolyte holes in the grinding wheel affected the ECMG process. The flow fields for grinding wheels A–D were simulated and analysed for an inlet pressure of 0.6 MPa. Because the electrolyte was exposed directly to the atmosphere once in the machining gap, we set the outlet pressure to zero. For this simulation, we chose the standard k–ε turbulence model and we compared and analysed the flow field in the observation section for different numbers of grinding-wheel holes. The simulation results are shown in Fig. 5.

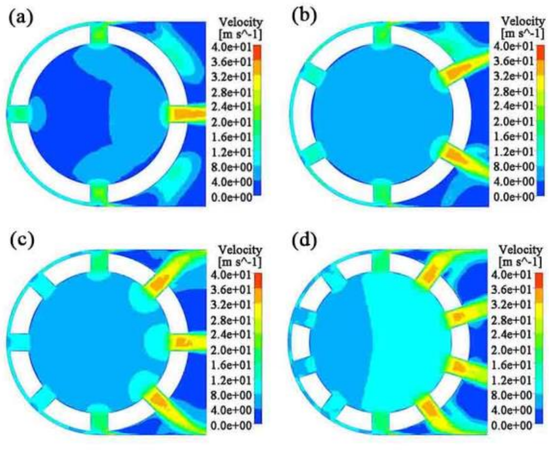

Figure 5. Flow fields for different numbers of electrolyte holes. (a) Number of holes: 20, inlet pressure: 0.6 MPa. (b) Number of holes: 30, inlet pressure: 0.6 MPa. (c) Number of holes: 40, inlet pressure: 0.6 MPa. (d) Number of holes: 50, inlet pressure: 0.6 MPa.

From the calculations, the average flow speed of electrolyte on observation sections A–D is 6.68 m/s, 8.25 m/s, 9.70 m/s and 10.96 m/s, respectively. It can be seen from Fig. 5 that when the electrolyte pressure is constant, the resistance to the electrolyte entering the machining region decreases with the number of grinding-wheel holes. Therefore, the average flow speed increases with the number of holes, as does the flow rate of electrolyte into the machining region. Because the machining gap is relatively narrow whereas the flow field to the right of the grinding wheel is open, the electrolyte in the machining gap experiences larger resistance. The electrolyte flows faster through the holes facing the machining gap (left) and slower through the holes facing the machined region (right). With fewer holes, the electrolyte flows faster in the machining gap, but the electrolyte flow path is currently too long to allow the processing products and Joule heat to be discharged in a timely manner.

Next, we investigated how changing the pressure affects the electrolyte. Because of experimental limitations, the maximum pressure at which electrolyte can be supplied in practice is 0.6 MPa. Therefore, we chose inlet pressures of 0.2 MPa, 0.4 MPa and 0.6 MPa with a constant zero outlet pressure and again used the standard k–ε turbulence model. Fig. 6 shows the flow fields for the three electrolyte inlet pressures, for which the average flow speed is 4.77 m/s, 6.87 m/s and 8.25 m/s, respectively. With the increase of the electrolyte pressure, the flow speed of the electrolyte in the machining region increases, which helps to promote the discharge of the electrolysis products in the machining gap and accelerates the process of ECMG.

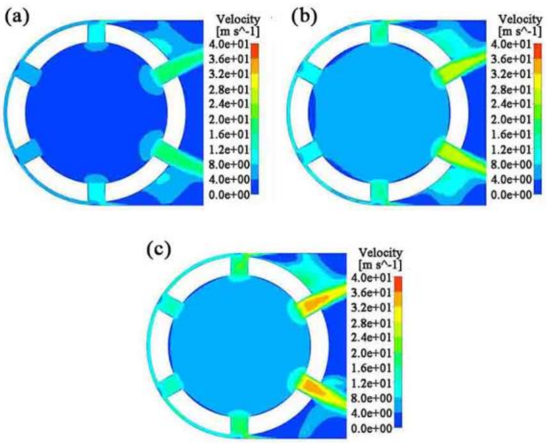

Figure 6. Flow fields for different inlet pressures. (a) Number of holes: 30, inlet pressure: 0.2 MPa. (b) Number of holes: 30, inlet pressure: 0.4 MPa. (c) Number of holes: 30, inlet pressure: 0.6 MPa.

In previous research on ECMG, in order to achieve a cutting depth of 3 mm, a grinding wheel with a single row of electrolyte holes was designed [19, 20]. However, when the cutting depth is increased to 10 mm, a single row of holes cannot provide sufficient electrolyte to the machining gap to give an acceptable MRR. A grinding wheel with holes distributed in multiple rows should provide a greater flow of electrolyte into the machining gap and thereby allow greater cutting depths to be achieved. Fig. 7 compares the flow field for a single row of holes with that for multiple rows, with the inlet pressure set at 0.6 MPa in both cases. The average flow velocities for single and multiple rows are 3.14 and 7.92 m/s, respectively, and thus the use of a grinding wheel with multiple rows of holes does indeed give a higher electrolyte flow rate.

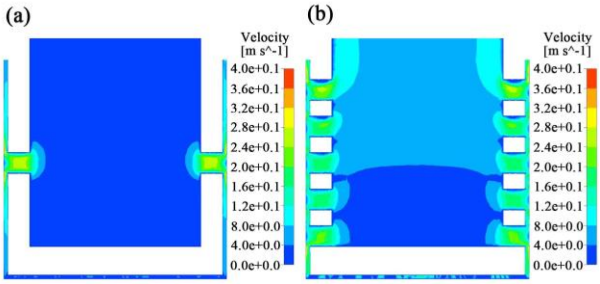

Figure 7. Flow fields for single and multiple rows of electrolyte holes. (a) Single row of holes. (b) Multiple rows of holes.

3. EXPERIMENTAL

Fig. 8 shows the experimental ECMG system schematically. It comprises four parts: the machining platform, the control system, the power supply system and the electrolyte system. On the machining platform, the grinding wheel is clamped to the spindle that is fixed to the Z sliding table, the workpiece is fixed on the cross sliding table, the grinding wheel can move and rotate in the working tank and the workpiece is clamped to the tank by the fixture. In the control system, the feed direction and feed rate of the grinding wheel are controlled by the X/Y/Z motors, the rotation rate is control by the spindle motor and these motors are driven by the computer. In the (direct current) power supply, the negative pole is connected to the spindle through a slip ring, the positive pole is connected to the workpiece and the circuit contains a Hall sensor to monitor the machining current in real time. In the electrolyte system, electrolyte is pumped out by the centrifugal pump through the rotary joint and the hollow spindle and is finally ejected from the electrolyte holes into the machining region; the used electrolyte is discharged into the waste tank and filtered before being returned to the electrolyte tank, and the thermostat and chiller are used to keep the electrolyte at a constant temperature.

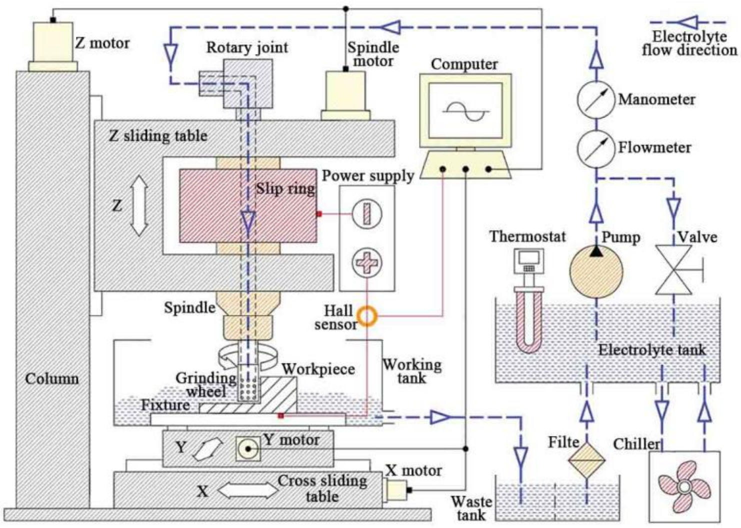

Figure 8. Schematic of experimental system.

Table 1. Material properties of GH4169 alloy workpiece.

Parameter	Value
Composition (wt%)	C: 0.038; Si: 0.16; Mn: 0.12; S: 0.001; P: 0.01; Ni: 52.75; Cr: 17.96; Al: 0.55; Cu: 0.022; Co: 0.018; Ti: 1.09; Mo: 3.05; Nb: 5.13; B: 0.002; Ta: 0.011; Fe: bal
Tensile strength σ_b (MPa)	1,310
Yield strength $\sigma_{0.2}$ (MPa)	1,025
Elongation δ_5	18
Section shrinkage ψ	26
Density (g/cm^3)	8.24

To obtain high MRR, we explored the maximum feed rate of grinding wheels A–D under different machining conditions. The wheel that gave the fastest feed rate was then chosen for the groove machining experiment. Table 1 lists the material properties of the GH4169 alloy (produced by Shanghai Lanzhu Super Alloy Materials Co., Ltd.) workpiece that we used, and Table 2 lists the machining conditions of the tests. We used a solution of 10wt% $NaNO_3$ as the electrolyte, which gives good machining precision as a type of passivizing electrolyte. ECM cannot be carried out normally if the electrolyte temperature is too high or too low, so we set the electrolyte temperature as 30°C based on previous experience. To get high grinding removal rate and prevent the electrolyte from being expelled from the machining region by the centrifugal force, we set the rotation speed of the grinding wheel as 1,000 rpm. Finally, to achieve high MRR, we set the cutting depth as 10 mm. To compare the effects of different values of applied voltage and electrolyte pressure on the machining effect of ECMG, we selected values of 15 V, 20 V, 25 V and 30 V and 0.2 MPa, 0.4 MPa and 0.6 MPa, respectively.

Table 2. Machining conditions for ECMG.

Parameter	Value
Workpiece size (mm)	100×100×15 (GH4169)
Grinding wheel type	A/B/C/D (20/30/40/50 holes)
Electrolyte type	$NaNO_3$ (10wt%)
Electrolyte temperature (°C)	30
Grinding-wheel rotation rate (rpm)	1,000
Cutting depth (mm)	10
Applied voltage (V)	15/20/25/30
Electrolyte pressure (MPa)	0.2/0.4/0.6

4. RESULTS AND DISCUSSION

4.1 Maximum feed rate testing

Fig. 9 shows the method used to measure the maximum feed rate of the grinding wheel. We began by cutting into the workpiece with the grinding wheel at a slow feed rate and then increased the feed rate by 0.1 mm/min every 5 min. We monitored the machining current in real time during the machining, and a short circuit indicated that the grinding wheel had exceeded the maximum feed rate for the machining conditions. As shown in Fig. 8, when the feed rate reached 2.0 mm/min, a short circuit occurred; the results show that the maximum feed rate for this machining was 1.9 mm/min. Table 3 lists the measured values of maximum feed rate.

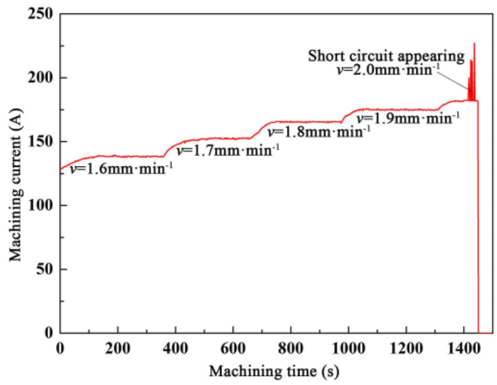

Figure 9. Method used to measure maximum feed rate.

Table 3. Measured values of maximum feed rate testing.

Group no.	Applied voltage (V)	Electrolyte pressure (MPa)	Maximum feed rates of each grinding wheel (mm/min)			
			A (20 holes)	B (30 holes)	C (40 holes)	D (50 holes)
1	15	0.2	1.0	1.1	1.3	1.4
2	15	0.4	1.3	1.3	1.5	1.5
3	15	0.6	1.5	1.6	1.6	1.6
4	20	0.2	1.1	1.3	1.5	1.4
5	20	0.4	1.4	1.6	1.7	1.6
6	20	0.6	1.7	1.9	1.9	1.7
7	25	0.2	1.2	1.5	1.6	1.5
8	25	0.4	1.5	1.8	1.8	1.7
9	25	0.6	1.7	2.1	2.0	1.8
10	30	0.2	1.3	1.7	1.7	1.7
11	30	0.4	1.6	2.1	2.0	1.9
12	30	0.6	1.8	2.3	2.2	1.9

In ECMG, the contribution of ECM to material removal is far greater than that of grinding, so the conductive area of the grinding wheel greatly influences the MRR. Because ECM occurs mainly in the contact region between the sidewall of the grinding wheel and the workpiece, we consider this semi-cylindrical region to be the conductive region. We calculated the conductive area of each grinding wheel as shown in Fig. 10. The conductive region becomes gradually smaller with the number of electrolyte holes. Fig. 11 compares the electrolyte flow rate under different machining conditions. As in simulation, the electrolyte flow rate increases with both the electrolyte pressure and the number of electrolyte holes.

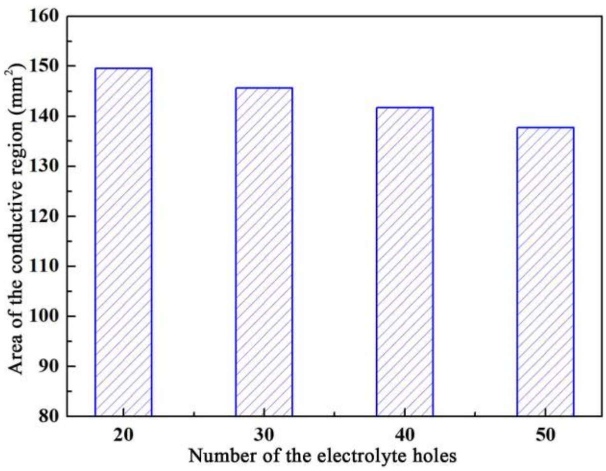

Figure 10. Comparison of conductive region areas.

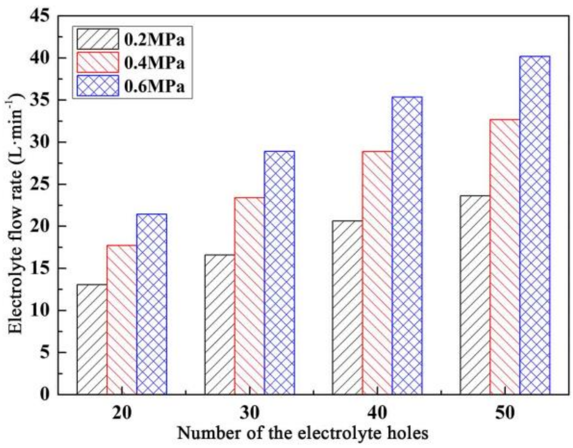

Figure 11. Comparison of electrolyte flow rates.

Fig. 12 compares the maximum feed rates of the grinding wheels under different machining conditions. The results show that increasing the applied voltage makes ECM more efficient and increases the feed rate of the grinding wheel. Furthermore, increasing the electrolyte pressure increases its flow rate in the machining region, allowing the processed products to be removed sooner and thereby accelerating ECMG machining.

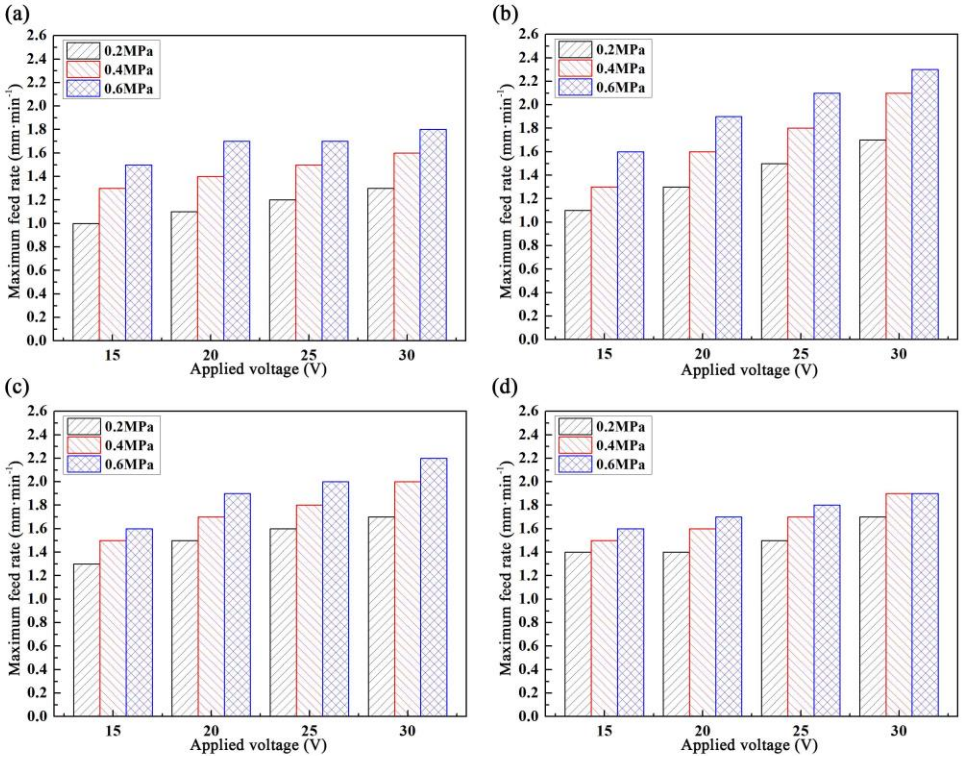

Figure 12. Comparison of maximum feed rates of different grinding wheels. (a) Grinding wheel A. (b) Grinding wheel B. (c) Grinding wheel C. (d) Grinding wheel D.

At low electrolyte pressure, a grinding wheel with more electrolyte holes delivers a higher feed rate because of the higher flow rate; when the electrolyte pressure is raised, the feed rate increase of a grinding wheel with fewer electrolyte holes is more obvious because of its larger conductive area. Too few electrolyte holes will lead to the failure of the electrolysis products to be discharged in time, and too many holes will decrease conductive area of the grinding wheel and weak the effect of ECM. Therefore, having too many or too few electrolyte holes in the grinding wheel will not give the highest maximum MRR for GH4169 alloy. The maximum feed rate (2.3 mm/min) was obtained with an applied voltage of 30 V and an electrolyte pressure of 0.6 MPa by using the grinding wheel with 30 electrolyte holes, a moderate number in this case.

4.2 Groove-machining experiment

To study how the machining conditions affect ECMG quality, we used grinding wheel B (30 holes) to machine experimental grooves. In this experiment, we selected six sets of machining conditions from Table 3 and machined grooves at the previously measured maximum feed rate. When the grinding wheel first cuts into the workpiece, the electrolyte flow in the machining region is poor. Therefore, in the groove machining, we set the feed rate of the grinding wheel initially as a low value (0.8 mm/min). When the grinding wheel had mostly cut into the workpiece (machining length: 5.5 mm), we increased the feed rate of the grinding wheel to the previously measured maximum value and set the total machining length as 25 mm. Table 4 lists the machining conditions of groove machining; the other machining conditions are as Table 2. Fig. 13 shows a sample groove machined in GH4169 alloy.

Table 4. Machining conditions for groove machining.

Group no.	Applied voltage (V)	Electrolyte pressure (MPa)	Maximum feed rate (mm/min)	Machining length (mm)
1	15	0.2	1.1	25
2	20	0.2	1.3	25
3	25	0.2	1.5	25
4	30	0.2	1.7	25
5	30	0.4	2.1	25
6	30	0.6	2.3	25

Figure 13. Groove machining sample.

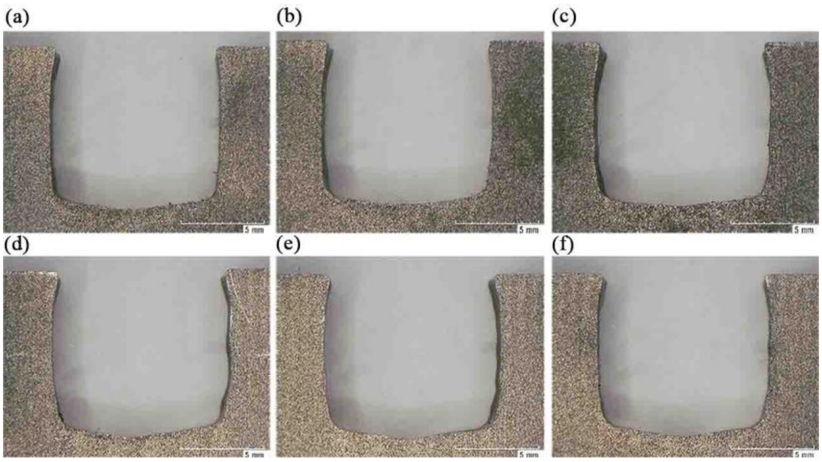

Figure 14. Comparison of groove sections under different machining conditions. (a) Group 1. (b) Group 2. (c) Group 3. (d) Group 4. (e) Group 5. (f) Group 6.

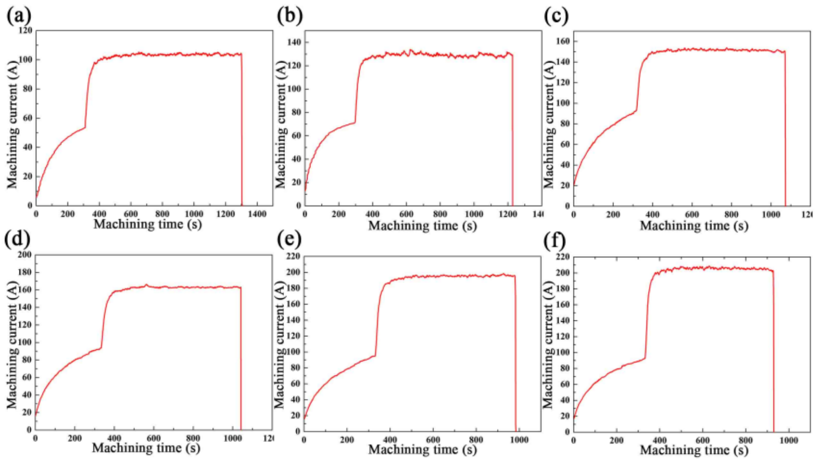

Figure 15. Comparison of machining currents under different machining conditions. (a) Group 1. (b) Group 2. (c) Group 3. (d) Group 4. (e) Group 5. (f) Group 6.

To observe the machining effect of different conditions, we cut grooves of a machining length of 15 mm by wire-electrode cutting and compared their cross sections. Fig. 14 compares the groove sections. In the groove machining, the machining current of each group was recorded by the current monitoring device. Fig. 15 compares the machining current in each group. The machining current rose slowly when the grinding wheel started to cut into the workpiece at a low feed rate. When the feed rate of the grinding wheel was raised to the maximum level, the machining current increased suddenly and then remained stable. We then calculated the current density of each group.

Next, we compared the MRR of each experimental group. We used a high-precision electronic balance (ME4002; Mettler-Toledo, SUI) to weigh the workpiece before and after the groove machining; the difference in weight was the amount of material removed by the machining. The MRR of each group is calculated as follows:

$$\mathrm{MRR} = \frac{m}{t_0}, \quad (5)$$

where m is the amount of material removed and t_0 is the machining time.

Table 5 lists the calculation results of the current density and MRR in each group, and Fig. 16 shows the relationship between the current density and MRR. The calculation results show that increasing the current density gave a higher MRR.

In ECM, increasing the current density can help to improve the material removal rate, and increasing cathode feed speed is an effective way to increase the current density [21]. From the experimental results, raising the applied voltage and the electrolyte pressure both can accelerate the feed rate of the grinding wheel and increase the current density. Therefore, increasing the applied voltage and the electrolyte pressure are effective ways to improve the MRR of ECMG. For an applied voltage of 30 V, an electrolyte pressure of 0.6 MPa and a grinding-wheel feed rate of 2.3 mm/min, the current density was 141.415 A/cm^2 and the ECMG MRR was 25.883 mg/s.

Table 5. Current density and material removal rate (MRR) of groove machining.

Group no.	Current density (A/cm^2)	MRR (mg/s)
1	70.879	13.998
2	87.981	17.772
3	103.709	21.099
4	118.363	23.960
5	134.890	25.082
6	141.415	25.883

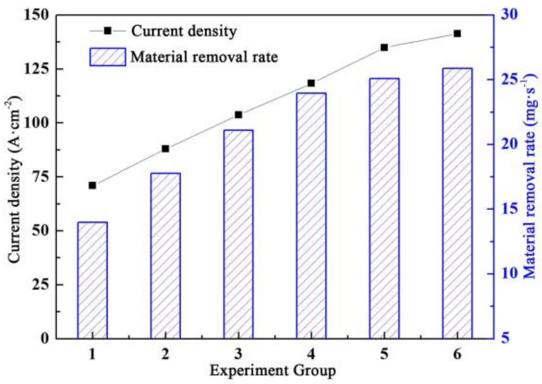

Figure 16. Relationship of current density and MRR.

In traditional grinding studies of nickel-based superalloy, because of the difficult cutting characteristics of the material, the cutting depth was usually less than 1mm [22,23]. Compared with traditional grinding, the cutting depth of ECMG is larger. In previous studies of ECMG of GH4169 alloy, the maximum cutting depth was 3 mm and the material removal rate was 5–8 mg/s, both of which values were restricted by the use of a single row of electrolyte holes in the grinding wheels [19,20]. With the use of the multiple-row design presented here, and with optimized machining conditions, the cutting depth is increased to 10 mm and the MRR is three to five times that in the previous studies of ECMG. Therefore, compared with a grinding wheel with a single row of electrolyte holes, the use of a wheel with multiple rows of holes can give higher machining efficiency.

To study the machining accuracy of ECMG, we used a three-coordinate measuring machine (Contura; Zeiss, GER) to measure the size of each machined groove surface. We selected 100 measuring points evenly on the two sides and the bottom surface of the groove section at a machining length of 15 mm. We set the upper surface of the workpiece as the datum plane and obtained the coordinates of the points on the groove profile. Fig. 17 shows a schematic of the three-coordinate measurement. Because the grinding wheel rotates clockwise and the electrolyte flows into the machining gap along one side (inflow surface) and flows out from the other side (outflow surface), the flow field differs at the two sides and the bottom surface of a machined groove. We calculated the average width, the average depth, and the overcut of the width and depth of each machined groove. To compare the flatness of the two sides and the bottom, we calculated the standard deviation (SD) of the transverse coordinates of the measuring points on the two sides of each groove and the longitudinal coordinates of the measuring point at the bottom of each groove. Table 6 lists the measurement results for machining accuracy.

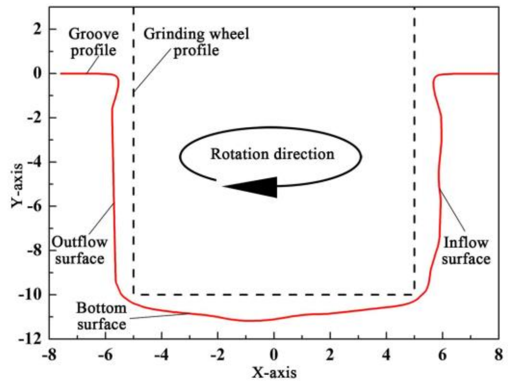

Figure 17. Schematic of groove measurement.

Table 6. Measured results for groove machining accuracy.

Group no.	Average width (mm)	Overcut width (mm)	Average depth (mm)	Overcut depth (mm)	SD of inflow surface (mm)	SD of outflow surface (mm)	SD of bottom surface (mm)
1	11.255	1.055	10.595	0.595	0.107	0.068	0.201
2	11.278	1.078	10.644	0.644	0.110	0.066	0.183
3	11.460	1.260	10.791	0.791	0.119	0.088	0.206
4	11.586	1.386	10.901	0.901	0.147	0.104	0.253
5	11.484	1.284	10.765	0.765	0.134	0.077	0.237
6	11.348	1.148	10.662	0.662	0.124	0.064	0.199

It can be seen from the measurement results that the overcut of the groove width is larger than that of the groove depth. This is because the two sides of the groove were facing the outlet of electrolyte holes, meaning that the electrolyte flow rate was higher at the sides and the electrolysis was stronger. And because there was no hole on the bottom surface of the grinding wheel, the flow rate of electrolyte on the bottom of the groove was lower, meaning that electrolysis was weaker there. By calculating the SD, the flatness of the sides and the bottom of the grooves are compared. In each machined groove, the outflow surface was flattest, followed by the inflow surface, with the bottom surface being the least flat, and the bottom of the groove was usually sunken. The analysis shows that the bottom was least flat because (i) it was electrolyzed repeatedly by the bottom of the grinding wheel, (ii) the centre of the bottom was corroded for the longest time. When the electrolyte had just entered the side of the machining gap, the flow field was disordered and the electrolytic corrosion rate was uneven on the inflow surface, leading to poor flatness. For the outflow surface, when the electrolyte flowed out of the machining gap, the flow rate became uniformly distributed, thereby improving the flatness.

We then used a roughness tester (Perthometer M1; Mahr, GER) to measure the roughness of the inflow surface, the outflow surface and the bottom surface of each machined groove. The roughness measurement results are listed in Table 7, and Fig. 18 shows the relationship between the roughness and the current density in the ECMG groove machining. To remove the residual black insoluble electrolysis products on the surface, the workpiece was treated by pickling before the measurement.

The measurement results show that the roughness of the machined groove surfaces decreased with current density. This is because the machined surface was electrolytically corroded again after grinding, leading to a change in surface roughness similar to that of ECM. In previous studies of ECM of nickel-based alloy, increasing the current density can make the machined surface uniformly corroded and reduce the surface roughness [24,25]. The measurement results prove that the conclusion is also applicable to the ECMG of GH4169 alloy. Compared to the bottom surface, the electrolyte flowed faster through the inflow surface and the outflow surface, therefore the degree of corrosion on the two sides was heavier and their surfaces were rougher.

Table 7. Measured results for groove machining roughness.

Group no.	Roughness of inflow surface (μm)	Roughness of outflow surface (μm)	Roughness of bottom surface (μm)
1	3.242	3.058	0.851
2	2.389	2.248	0.786
3	1.952	1.868	0.612
4	1.719	1.656	0.556
5	1.590	1.575	0.543
6	1.489	1.435	0.527

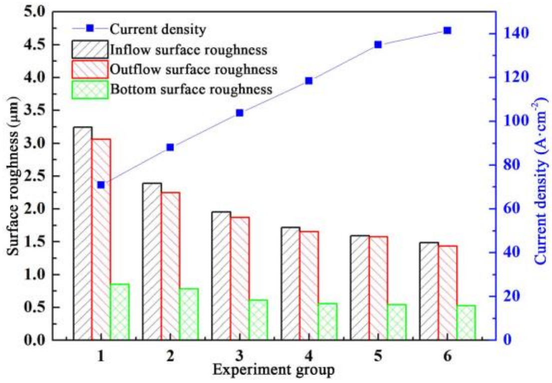

Figure 18. Relationship of current density and roughness.

5. CONCLUSIONS

1) We designed four grinding wheels with different numbers of electrolyte holes and simulated the flow field in the ECMG machining region. The results show that increasing the number of electrolyte holes and raising the pressure of the electrolyte improve the flow rate in the machining region and accelerate the ECM.

2) We measured the maximum feed rates of the four grinding wheels under different applied voltages (15–30 V) and electrolyte pressures (0.2–0.6 MPa). The feed rate can be increased by increasing the values of these two machining conditions. In addition, because of the influence of the conductive area and the flow rate, the maximum feed rate can be obtained by using a grinding wheel with a moderate number of electrolyte holes (30 in this case).

3) In ECMG groove machining, increasing the current density can reduce the roughness of the machined surface while increasing the MRR. Because of the differing flow fields at each machined surface of a groove, the outflow surface is flattest, followed by the inflow surface, with the bottom surface being the least flat.

ACKNOWLEDGEMENTS
This work was supported by the National Natural Science Funds of China (grant no. 51323008) and the Funding of Jiangsu Innovation Program for Graduate Education (grant no. KYLX16_0316).

References

1. Z. R. Wu, F. L. Liu, X. Li, L. Fang and Y. D. Song, *Adv. Mech. Eng.*, 9(11) (2017) 1.
2. Y. L. Pu, S. Z. Kou, Z. D. Zhang, T. W. Dong, X. F. Guo and H. X. Qu, *China Foundry*, 14(4) (2017) 244.
3. X. C. Zhang, H. C. Li, X. Zeng, S. T. Tu, C. C. Zhang and Q. Q. Wang, *Mater. Sci. Eng. A*, 682 (2017) 12.
4. R. Z. Wang, X. C. Zhang, J. G. Gong, X. M. Zhu, S. T. Tu and C. C. Zhang, *Int. J. Fatigue*, 97 (2016) 114.
5. X. Li, S. Ma and F. J. Meng, *Chin. J. Aeronaut.*, 28(5) (2015) 1539.
6. P. F. Guo, X. Lin, J. Q. Li, Y. F. Zhang, M. H. Song and W. D. Huang, *Corrosion Sci.*, 132 (2018) 79.
7. A. Ruszaj and M. Zybura-Skrabalak, *J. Mater. Process. Technol.*, 109(3) (2001) 333.
8. W. Natsu, T. Ikeda and M. Kunieda, *Precision Eng.*, 31(1) (2007) 33.
9. W. Vanderauwera, M. Vanloffelt, R. Perez and B. Lauwers, *Proc. CIRP*, 6 (2013) 356.
10. X. L. Fang, N. S. Qu, Y. D. Zhang, Z. Y. Xu and D Zhu, *J. Mater. Process. Technol.*, 214(3) (2014) 556.
11. S. Niu, N. S. Qu, S. X. Fu, X. L. Fang and H. S. Li, *Int. J. Adv. Manufact. Technol.*, 93(5–8) (2017) 2123.
12. J. Kozak, A. F. Budzynski and P. Domanowski, *J. Mater. Process. Technol.*, 76(1–3) (1998) 161.
13. J. Kozak, *J. Mater. Process. Technol.*, 109(1–3) (2001) 354.
14. J. Kozak, M. Chuchro, A. Ruszaj and K. Karbowski, *J. Mater. Process. Technol.*, 107(1–3) (2000) 283.
15. S. Hinduja and J. Pattavanitch, *CIRP J. Manufact. Sci. Technol.*, 12 (2016) 79.
16. R. Mahdavinejad and M. Hatami, *J. Mater. Process. Technol.*, 202(1) (2008) 307.

17. A. F. Tehrani and J. Atkinson, *Proc. IMechE B: J. Eng. Manufact.*, 214(4) (2000) 259.
18. N. S. Qu, Q. L. Zhang, X. L. Fang, E. K. Ye and D. Zhu, *Proc. CIRP*, 35 (2015) 16.
19. H. S. Li, S. X. Fu, Q. L. Zhang, S. Niu and N. S. Qu, *Chin. J. Aeronaut.*, 31(3) (2018) 608.
20. H. S. Li, S. Niu, Q. L. Zhang, S. X. Fu and N. S. Qu, *Sci. Rep.*, 7(1) (2017) 3482.
21. L. Tang and S. Yang, *Int. J. Adv. Manufact. Technol.*, 67(9-12) (2013)2909.
22. Z. D. Shi, A. Elfizy, B. St-Pierre and H. Attia, *Int. J. Abrasive Technol.*, 5(1) (2012) 1.
23. W. F. Ding, J. H. Xu, Z. Z. Chen, H. H. Su and Y. C. Fu, *Chin. J. Aeronaut.*, 23 (2010) 501.
24. F. Klocke, M. Zeis and A. Klink, *Key Eng. Mater.*, 504-506 (2012) 1237.
25. A. A. Nayak, S. Gangopadhyay and D. K. Sahoo, *J. Manufac. Process.*, 23 (2016) 269.